HHS Public Access

Author manuscript

Exp Eye Res. Author manuscript; available in PMC 2023 October 01.

Published in final edited form as:

Exp Eye Res. 2022 October ; 223: 109215. doi:10.1016/j.exer.2022.109215.

Age Differential Response to Bevacizumab Therapy in Choroidal Neovascularization in Rabbits

Van Phuc Nguyen[a], **Jessica Henry**[a], **Josh Zhe**[a], **Quynh Kieu**[a], **Wei Qian**[d], **Yingbin Fu**[c], **Xueding Wang**[b], **Yannis M. Paulus**[a,b,*]

[a]Department of Ophthalmology and Visual Sciences, University of Michigan, Ann Arbor, MI 48105, USA

[b]Department of Biomedical Engineering, University of Michigan, Ann Arbor, MI 48105, USA

[c]Department of Ophthalmology, Baylor College of Medicine, Houston, TX 76706, USA.

[d]IMRA Inc., Ann Arbor, MI 48105, USA

Abstract

Choroidal neovascularization (CNV) in young rabbits has been shown to have a rapid, robust response after treatment with bevacizumab, an anti-vascular endothelial growth factor (VEGF) medication. This investigation evaluates an age differential response to bevacizumab in older populations of rabbits using multimodal high resolution molecular imaging. Young (4 months old) and life span (14 months old) rabbits were given subretinal injections of Matrigel and VEGF to produce CNV. All CNV rabbit models were then treated with a bevacizumab intravitreal injection. Rabbits were then monitored longitudinally using photoacoustic microscopy (PAM), optical coherence tomography (OCT), color photography, and fluorescence imaging. Chain-like gold nanoparticle clusters (CGNP) conjugated with tripeptide arginylglycylaspartic acid (RGD) was injected intravenously for molecular imaging. Robust CNV developed in both young and old rabbits. After intravitreal bevacizumab injection, fluorescence signals were markedly decreased 90.13% in the young group. In contrast, old rabbit CNV area decreased by only 10.56% post-bevacizumab treatment. OCT images confirmed a rapid decrease of CNV in the young group. CGNPs demonstrated high PAM signal in old rabbits and minimal PAM signal in young rabbits after bevacizumab, indicating CNV regression. There is a significant difference in response to intravitreal bevacizumab treatment between young and old rabbits with CNV which can be monitored with multimodal molecular imaging. Old rabbits demonstrate significant persistent disease activity. This represents the first large eye model of persistent disease activity of CNV and could serve as the foundation for future investigations into the mechanism of persistent disease activity and the development of novel therapies.

[*]**Corresponding Author: Yannis M. Paulus, M.D., F.A.C.S.**, Department of Ophthalmology and Visual Sciences, Department of Biomedical Engineering, University of Michigan, 1000 Wall Street, Ann Arbor, MI 48105, USA, ypaulus@med.umich.edu.

Disclosures: None of the authors has a conflict of interest relevant to this paper.

Keywords

anti-VEGF resistance; choroidal neovascularization; persistent disease activity; photoacoustic microscopy; OCT

1. Introduction

Choroidal neovascularization (CNV) occurs in several diseases, including a major cause of vision loss and blindness in the United States and worldwide: age-related macular degeneration (AMD) (Cheung et al., 2017; Cohen et al., 1996; Ferris et al., 1984). In 2020, 196 million people were estimated to be diagnosed with AMD, 11.3 million of which suffer from advanced AMD (Buckle et al., 2015; Mukesh et al., 2004; Nguyen et al., 2018; Rein et al., 2009; Solomon et al., 2014; Stem et al., 2018; Wong et al., 2014). Although anti-VEGF therapy is the new standard in CNV treatment, a significant number of patients have suboptimal response to this therapy or develop resistance over long-term use. One common issue is persistent disease activity (PDA). The comparison of AMD treatments trial (CATT) found persistent fluid in 53% of patients treated monthly with ranibizumab, and 71% of those treated with bevacizumab (Martin et al., 2011). After 5 years of monthly anti-VEGF therapy, 20% of patients become legally blind and an additional 30% of individuals have some degree of vision loss (Maguire et al., 2016).

Despite widespread research, the intricate details of CNV formation remain a field of dynamic exploration. Significant limitations have plagued the majority of animal models that attempt to replicate CNV development. Many CNV models that are successful use physical devastation of the RPE layer (retinal pigment epithelium) or Bruch's membrane. A common physical destruction method utilizes lasers to induce CNV in rodents (mice and rats) or larger animals such as monkeys and pigs (Kiilgaard et al., 2005; Miller et al., 1990; Semkova et al., 2003; Shah et al., 2015). Current attempts to reproduce CNV using laser photocoagulation in rabbits have not yet been successful; however reports have demonstrated that artificial sub-RPE injection can create the formation of CNV in rodents and rabbits (Cao et al., 2010).

Preclinical animal models such as rabbits have been widely utilized due to having relatively large eyes that share physiologic parameters similar to those seen in humans. These likenesses consist of the eyeball size and shape, optical system, choroidal blood supply, anterior segment structures, posterior segment structures, biomechanical, and biochemical features. The rabbit eye has an 18.1 mm axial length, or nearly 80% that of humans, which is approximately 23 mm, whereas mice have only 3.2 mm axial length, or only 13% that of humans, while rats have roughly a 5.98 mm axial length. Furthermore, numerous physiologic physiotherapy methods and apparatus designed for ocular applications in humans are able to be implemented in rabbits' eyes with slight modification (Ahn et al., 2016; Del Amo and Urtti, 2015; Hasumura et al., 2000). Much is known about the rabbit choroidal vasculature, and it shares many similarities to human choroidal vasculature (Abdo et al., 2017; Reichenbach et al., 1991a; Reichenbach et al., 1991b).

In 2006, a novel method using subretinal administration of mixed VEGF and Matrigel solution into the rabbit's retina to induce CNV was developed that is reliable, reproducible, and sustainable (Qiu et al., 2006). This method has also been demonstrated in adult Sprague-Dawley rats (Cao et al., 2010) and mice (Johnson et al., 2008). Matrigel is primarily composed of collagen IV, laminin, entactin/ nidogen, growth factors, and heparin sulfate proteoglycans. Liquid Matrigel, usually at 4°C, is injected into tissue where it solidifies after acclimating to the surrounding tissue temperature due to its solidified at 37 °C, thus trapping the growth factors. These growth factors are slowly released, permitting prolonged development of CNV. On the other hand, a major limitation of these rabbit animal models is that they fail to recapitulate persistent disease activity (PDA) and are readily responsive to anti- VEGF therapy (Lima et al., 2018). Previous studies have reported successful repression of angiogenesis after bevacizumab injection among young rabbits, but no study was conducted to investigate the differential response to treatment between young and old rabbits (Ameri et al., 2007). Rigorous studies have demonstrated a robust PDA model in old mice compared to young mice using laser-induced CNV (Mettu et al., 2021; Zhu et al., 2020), and thus we hypothesized that old rabbits might also serve as a model of PDA.

2. Materials and Methods

2.1 Integrated PAM and OCT system

In our previous publications we described an integrated optical coherence tomography (OCT) and photoacoustic microscopy (PAM) system (Tian et al., 2017b; Tian et al., 2018; Zhang et al., 2020a; Zhang et al., 2018; Zhang et al., 2020b). PAM is a new ophthalmological imaging modality based on the creation of ultrasound waves by the absorption of laser energy of retinal tissues such as melanin or hemoglobin. For PAM, a photoacoustic signal (PA) was induced by generating 1000Hz laser with a 3–5 ns pulse width from an optical parametric oscillator (OPO). The OPO was pumped by Nd:YAG laser (NT-242, Ekspla, Vilnius, Lithuania). The light beam was filtered and collimated to form a circular shape of 2 mm. This beam was then delivered to the corneal surface through complex optics system including scanning head, scan lens and ophthalmic lens before focused on the fundus with an approximately 20 μm. A custom-made, 27 MHz center frequency, ultrasonic transducer was utilized to receive the laser-induced PA signal from endogenous chromophores (Optosonic Inc., Arcadia, CA, USA). An amplifier was applied to amplify the PA signal (gain 57 dB, AU-1647, L3 Narda-MITEQ, NY). These signals were then captured using a 200 MS/s digitizer (Signatec Inc., Newport Beach, CA). Reconstructed three-dimensional and two-dimensional PAM images of blood vessels in the retina were produced using the recorded data. To acquire OCT imaging, the system from a Ganymede-II-HR OCT system (Thorlabs, Newton, NJ) was modified as described in previous study (Tian et al., 2017a). Two superluminescent diodes (SLDs) with a central wavelength of 905nm was used to excite the tissues. The light from the light source was produced by a single node fiber and was later split into sample and reference arms. The OCT was integrated with the PAM system. The imaging depth up to 1.9 mm can be achieved with this combined system.

2.2 Animal experiments

All animal studies followed the guidelines of the ARVO (the Association for Research in Vision and Ophthalmology) Statement on the care and use of laboratory animals in ophthalmic and vision research after approval by the University of Michigan Institutional Animal Care and Use Committee (IACUC, protocol PRO00010388, PI Paulus). The New Zealand White rabbits aged 4 and 14 months old (2.2–3.8 kg) were kindly donated by the University of Michigan Center for Advanced Models and Translational Sciences and Therapeutics (CAMTraST).

A pulse oximeter was used to record and monitor rabbit's conditions such as heart rate, temperature, and respiratory rate (V8400D Capnograph & SpO2 Digital Pulse Oximetry, Smiths Medical, MN, USA) before every experiment and every 15 minutes during the experiment until the animals became fully alert and ambulatory. Prior to the experiment, each rabbit received two medications for anesthesia (ketamine (40 mg/kg, 100 mg/mL) and xylazine (5 mg/kg, 100 mg/mL)) by intramuscular route. Anesthesia was maintained during the experiment by providing the animals 1/3 dose of ketamine every additional 45 minutes.

2.3 Subretinal injection model

A mixed solution of Matrigel (Corning, NY, USA) and VEGF (Shenandoah Biotechnology, Warwick, USA) was prepared for subretinal injections as described in detail previously (Li et al., 2019). Briefly, Matrigel (20 μL) was mixed with VEGF (7.5 mL; 100 μg/mL) and kept in the refrigerator at 4 °C. Tropicamide 1% ophthalmic (Akorn, Decatur, IL, USA) and phenylephrine hydrochloride 2.5% ophthalmic (Bausch & Lomb Pharmaceuticals, Tampa, FL, USA) were applied on each eye to dilate the pupils. Surgical scissors were used to remove the superior rectus muscle. A 26G needle was utilized to create a scleral tunnel at a distance of 3.5 mm from the limbus to the posterior segment. A silicone contact lens was mounted on the cornea of the rabbit eye (Volk Optical Inc., Mentor, OH, USA). The surface of the contact lens was prepared with Gonak gel (Akorn, Lake Forest, IL, USA) for coupling between the incident light and the cornea. Using a 30G Hamilton needle, the tip of the 50 mL syringe containing 27.5 μL of Matrigel and VEGF (M&V) mixture was inserted into the eye through the scleral hole. Under the operating microscope, the tip was gently inserted until it reached the retinal tissue. The M&V mixture was injected into the subretinal space using real-time OCT image guidance, and then the syringe was slowly retracted. The injection area was followed up over 1 month using PAM, OCT, color, and FA imaging.

2.4 Anti VEGF- treatment

A dose of bevacizumab (Avastin, 25 mg/mL, 50 μL; Fargon Sterile Services, KS, USA) was intravitreally injected 3 days post administration of VEGF at 3.5–4.0 mm from the limbus to the posterior segment into the rabbit vitreous cavity using a 30G ½ inch needle under a microscope.

2.5 Post bevacizumab treatment monitoring

All rabbits with CNV models were evaluated at day 3 after VEGF injection and after bevacizumab treatment at day 3, 7, 14, 21, and 28. Comprehensive ophthalmoscopic

examination, fluorescein angiography (FA), PAM, OCT, and color imaging were used to evaluate the treatment efficiency.

2.5.1 Comprehensive ophthalmoscopic examination—Comprehensive ophthalmoscopic examinations were employed on all rabbit after administration at days 3, 7, 14, 21, and 28. Slit lamp biomicroscope was used to examine for evidence of eye inflammation, infection, cataract, or erythema or edema at the injection site.

2.5.2 Color and fluorescein angiography (FA) imaging—Imaging of retinal blood vessels and CNV before and after bevacizumab treatment was generated using 50° color fundus photography (Topcon 50EX, Topcon Corporation, Tokyo, Japan). These vessels as well as neighboring vessels were captured at different angles and positions in the eye to monitor the impact of bevacizumab in specific portions. Specifically, we focused on the optic nerve, the inferior retina, the superior retina, the temporal and nasal medullary ray. FA was captured in tandem with fundus system to examine the CNV and vasculature. 0.2 mL of sodium fluorescein solution (10% fluorescein) was administrated into the marginal ear (Akorn, Lake Forest, IL, USA). Images were captured serially after the administration and were continued to be captured for up to 20 minutes.

2.5.3 Molecular Imaging using Gold Nanoparticles—Chain-like clusters gold nanoparticle clusters (CGNPs) were employed in order to boost the sensitivity of OCT and PAM imaging as described previously (Nguyen et al., 2021c). In brief, discrete colloidal GNPs (~20 nm) were manufactured using femtosecond ablation laser system (FCPA μJewel D-1000, IMRA America, Ann Arbor, MI). The fabricated GNPs have naturally negatively charged without using any capping agents to maintain their stability. Two different pentapeptides including cysteamine and Cys-Ala-Leu-Asn-Asn (CALNN) peptides were applied for assembly of discreet GNPs into chain-like GNP clusters (CGNP). These CGNP were conjugated with RGD, a peptide that localizes to integrin present in angiogenesis but not in normal vasculature. The distribution of CGNPs during angiogenesis is confirmed using two different rabbit groups. To demonstrate the efficacy of CGNPs, these clusters were used to target CNV by accumulating at the diseased sites caused by CNV.

2.5.4 PAM and OCT *in vivo* imaging—To observe the treatment efficiency, we further performed OCT and PAM imaging on the treated animals using our custom-built multimodality imaging system (Nguyen et al., 2020; Nguyen et al., 2021a; Nguyen et al., 2021b; Nguyen et al., 2021c; Tian et al., 2018). Rabbits (N=9) were split into 3 groups: control group (without treatment with bevacizumab) and bevacizumab treatments for 4 and 14-months old group. After 28 days of bevacizumab therapy, all animals were administrated with 400 μL (5 mg/ml) of CGNPs via intravenous injection of the marginal ear vein. CNV were monitored pre and post the administration of CGNPs. In order to achieve the PAM and OCT images, the rabbits under anesthesia were positioned on couple separate stages to reduce movement artifacts. In order to maintain the coupling between the ultrasound transducer and the conjunctiva, balanced salt solutions (BSS) were provided on the cornea every minute. During the experiment, the body temperature was kept stable using a water circulating heating blanket. The PAM images were captured using the excitation wavelength

of 578 nm to image the choroidal and retinal vascular networks and 650 nm to image the nanoparticles which localize to CNV. The location of CNV was scanned with an area of approximately 4.5×4.5 mm^2 with a resolution of 256×256 pixels. Three-dimensional PAM images were rendered using Amira 6.0 (Visualization Sciences Group).

2.6 Histological and Immunohistochemistry Analysis

Twenty-eight days after bevacizumab treatment, rabbits were sacrificed, and their retinal vessels were examined using histological analysis. Euthanasia was performed by intravenously injecting of 0.22 mg/kg (50 mg/mL) Euthanasia pentobarbital solution (Euthanasia Special, Intervet Inc., Madison, NJ, USA). The eyeballs and organs including heart, spleen, lung, liver, and kidney were harvested for histological analysis. These tissues were fixed in 10% neutral buffered formalin (VWR, Radnor, PA, USA) for 24 hours. Davidson's fixative solution was utilized to maintain the retinal integrity while the eyeball was kept in the solution for 24 hours (Electron Microscope Sciences, PA, USA). In the next day, these eyeballs were soaked in 50% alcohol solution for at least 8 hours (Fisher Scientific, PA, USA). After that, these tissues were kept at room temperature and transferred to a 70% alcohol solution for another 24 hours. The fixed tissues were then embedded in paraffin and a transverse section was performed using a Leica autostainer XL (Leica Biosystems, Nussloch, Germany). This was followed by hematoxylin and eosin (H&E) staining.

We further performed immunohistochemistry to examine the development of CNV using anti-alpha smooth muscle actin (α-SMA) antibody. Immunofluorescence was performed to stain macrophages appeared at CNV walls using Anti-CD163 antibody (ab156769, Abcam, Burlingame, CA, US). Two fluorescence-conjugated secondary antibodies including goat anti-mouse IgG antibody Alexa Fluor 488 and goat anti-rabbit IgG antibody Alexa Fluor 555 were used to incubate the samples for 60 min in the dark environment and kept the sample at temperature of 37 °C (Cell Signaling Technology, Boston, MA, USA). Mounting medium with DAPI was used to cover these slides with cover slip (Vector Laboratories, Burlingame, CA, USA). The H&E and IHC slides were examined under microscope (DM600, Leica Biosystems, Nussloch, Germany). High resolution images were acquired with the BF450C camera to capture H&E color image and the BFX365C camera to obtain the immunofluorescence images.

2.7 Fluorescent Signal and Vessel Density Quantification

To evaluate the efficiency of treatment effect between treatment groups, fluorescent intensity (FI) and vessels density (VD) were calculated at each time point. We first segmented the CNV area using MATLAB image segmentation algorithm. First, the image contrast of the fluorescent images was enhanced using adaptive histogram equalization function. Then, the boundary of the fluorescent leakage area was extracted using edge detection function. The FI was calculated as a mean value from each pixel within the extracted area. Normalized FI was applied for each time point. The pretreatment time point was set as 1 and a relative value was calculated for each time point post treatment. The VD was measured by counting each pixel along with the extracted fluorescent leakage area. The VD was determined by normalizing the VD before treatment to the VD after treatment.

2.8 Statistical Analysis

Statistical analysis was implemented using a one-way ANOVA method with the Tukey's post hoc test to determine statistical significance between treatment groups. This analysis was performed using Origin software (OriginLab Corporation, MA, USA). Data were expressed as averages ± standard deviation and significantly difference between treatment group was considered when $p < 0.05$

3. Results

3.1 Bevacizumab inhibition of subretinal injection of VEGF induced CNV in rabbits

All the rabbits injected with subretinal Matrigel and VEGF developed florid CNV and active exudation after 3 days. Figure 1 shows the color fundus and fluorescein angiography (FA) images of the CNV without bevacizumab treatment as a control. The results demonstrate that retinal vascular tortuosity near the subretinal injection site developed in all the treated eyes. During follow-up, there was no evidence of opacities, hemorrhage, or vitreous inflammation visualized in all treated animals. The location and boundary of CNV were clearly observed on the late phase FA images. We found that there was no significant reduction in fluorescein leakage over time, confirming that CNV persisted and was stable.

To assess the CNV treatment effects of bevacizumab in young and aged rabbits, we performed treatment on two groups of rabbits that were 4 months old and 14-months old as shown in Figures 2–3. At 3 days post injection, all Matrigel and VEGF-injected eyes demonstrated fluorescein leakage at the site of injection in all experimental eyes. These leaking hyperfluorescent zones appeared to be similar between the 4 and 14 month old groups before treatment with bevacizumab. In some rabbits, retinal hemorrhages occurred at the injection site as shown in Figure 3, but no deep choroidal or suprachoroidal hemorrhages were detected. No additional complications were noted with no cases of infection (endophthalmitis) or cataract formation.

After bevacizumab treatment, the fluorescein leakage intensity and area were significantly different between the three treatment groups. There was no significant reduction in fluorescein leakage intensity and area observed in the 14-month-old and control groups (Fig. 2). The subretinal hyperfluorescent leaking area slightly regressed at day 3 post bevacizumab treatment and then gradually increased and stabilized in the 28-day follow-up period. No significant change in hyperfluorescent leaking was noted on the control group. In contrast, the fluorescein leakage intensity and area were significantly decreased at day 3 post treatment with bevacizumab and continued to decrease over time found in the 4-month-old group (Fig. 3). No evidence of increased fluorescein signal was found at day 28, confirming that CNV had regressed and persistently remained regressed in the 4-month-old group. Post image processing was performed in order to extract the boundary of fluorescein leakage (Figure S1). The fluorescein intensity and margins were measured as shown in Figure 4. Figure 4a and 4c show the late phase FA images before segmentation. The CNV areas were extracted and displayed on the overlay segmented images (Figure 4b and 4d). The segmented CNV areas extracted from 4-months old group were significantly reduced in compared to the 14-months old group (red marker). Figure 4e–f illustrate the

panel of the quantification fluorescent intensity and vessels density (VD) achieved from two different treatment groups and control group. The data indicated a trend of decreasing CNV leakage area at day 3 regarding of the 14 months old group (red line). Growth of the fluorescein leaking area over time was observed on 14 months old and control groups (black and blue lines). Compared to control and 14 months old groups, the CNV lesion area on the 4-month old group reduced 70.28 % (normalized vessels density = 0.3±0.15 (a.u.) for 4-month old group vs. 0.94±0.12 (a.u.) and 0.88±0.17(a.u.) for 14 month old and control groups, respectively) with the fluorescein leakage intensity reducing 9 to 10-fold (normalized fluorescein intensity is 0.1±0.05 (a.u.) for 4-month old group vs. 0.89±0.11 (a.u.) and 0.94±0.11 (a.u.) for 14 month old and control groups, respectively).

3.2 Non-invasive, high resolution photoacoustic microscopy (PAM) evaluation

PAM imaging was further performed to evaluate the presence of CNV in rabbit eyes after treatment with bevacizumab. After 28 days of bevacizumab therapy, all the treated animals were intravenously injected with CGNPs conjugated with RGD peptide (400 μL; 5 mg/mL), which localizes to integrin present in CNV. PAM images were taken pre and post CGNPs administration at 24 h (Figure 5). These images were achieved at 578 and 650 nm under a laser illumination of about 80 nJ. Figure 5b and 5f show the PAM images attained at 578 nm along the targeted regions demonstrated in Figures 5a and 5e. Retinal morphology and choroidal vasculature was distinctly detected on the PAM images with great contrast and spatial resolution. There were no signals perceived on the PAM images taken at 650 nm on the 4 months old group to determine the location of the CGNP (Figure 5c). At 24 h post CGNPs administration, the PAM image achieved at 650 nm on the 14 months old group showed strong PAM signal (green color), indicating the targeting of CGNPs at CNV (Fig. 5g). In contrast, minimal PAM signal was detected on the MIP PAM graphs achieved from the 4-month group as illustrated on Fig. 5c. This illustrates that CNV was almost gone after treatment with bevacizumab in young rabbits. The overlay PAM images clearly show the position of CNV in the retina (Fig. 5h). The PAM signal extracted from the aged group (14 months old) was significantly different and exhibited 18-fold stronger than the young group (4 months old) according to ANOVA analysis with *$p < 0.001$ ($n = 3$ for each group).

3.3 *In vivo* OCT imaging Analysis

OCT imaging was also employed to visualize the development of CNV lesions as well as monitor treatment progression. Before bevacizumab treatment, the OCT images showed different layers of the choroid and retinal tissues including retinal vessels, choroidal vessels, retinal pigment epithelium, and sclera as well as newly formation CNV (red arrows) in the subretinal space (Figs. 6a and 6c). After bevacizumab treatment, the 4-month-old group showed a significant reduction of CNV which correlated with our histologic results (Figure 6b). In comparison with before treatment, the CNV thickness was reduced by approximately 82.83% ($n=3$, $p<0.001$). In addition, the normalized CNV area was decreased by about 83.34% in comparison to pre-treatment ($n=3$, $p<0.001$). However, no significant difference was found in the 14-month-old group ($n=3$, $p>0.05$), confirming that bevacizumab has minimal impact on the old rabbits (Fig. 6d). This result agrees with the results reported by Zhu *et al.*(Zhu et al., 2020) in a mouse laser-induced CNV model. Figure 6e–f show the 3D OCT images achieved from both the 4-month-old group (Figure 6e) and 14-month-old

group (Figure 6f). These 3D OCT images illustrated the entire retina's architecture including retinal vessels, choroidal vessels, and nerve fiber layer as well as the dynamic changes in the retina's structure at the location of developed CNV. At the CNV development, choroidal vessels were reduced due to the side effects caused by Matrigel, which is consistent with the color fundus image shown in Figures 1–3.

3.4 Histological and Immunohistochemistry (IHC) Evaluation

Histological and IHC analysis were obtained from the euthanized rabbits at day 28 post bevacizumab treatment. Histological evaluation shows retinal disorganization and confirms the presence of newly developed CNV beneath the neurosensory retina, matching the regions of fluorescent leakage found in FA images demonstrated in both control and treated groups (Figs. 7a–c). In some areas, CNV was identified to begin from the choroid layer and spread into the subretinal space through ruptures in Bruch's membrane. We observed a massive loss of the outer nuclear layer (ONL) and photoreceptors in all treatment groups. Neovascularization after bevacizumab treatment in the young rabbit group was less than in the aged rabbit group (Figs. 7b & c). The histological analysis also shows no evidence of nuclei morphology changes, confirming no toxic effect associated with bevacizumab treatment. α-SMA was highly expressed in the 14-month-old group, whereas the α-SMA was less expressed at the CNV lesion obtained from the 4-month-old group (Figs. 7d–f). To assess the expression of CD163 appeared at the location of experimental CNV, we implemented immunofluorescence analysis. The immunofluorescence-stained images demonstrate that few CD163-possitive macrophages observed in the retina and choroid layers obtained from the control rabbit. In contrast, most of the CD163-possitive macrophages were detected in subretinal spaces around the CNV lesion and in some location in the inner layer in both young and life span rabbits as marked by red arrows.

4. Discussion

This study demonstrates how young and old rabbits with subretinal injection of Matrigel/VEGF-induced CNV respond to bevacizumab treatment and delineate differences in response between the two age groups. Our results showed that at 1, 2-, 7-, 14-, and 28-days post-treatment, there was a significant reduction in neovascularization among the young rabbits but minimal change in CNV among the old rabbits (Figs. 2–4). These results are consistent with the published data in mice (Zhu et al., 2020) and support the species independence of age-dependent resistance of CNV to anti-VEGF therapy. This result is highly significant because it demonstrates the first large mammalian AMD model of anti-VEGF resistance, which is invaluable for further mechanistic and translational studies. This is noteworthy since the U.S. Food and Drug Administration (FDA) recommendations necessitate that the efficacy of a pharmaceutical product must be demonstrated in rodent and one non-rodent, and rabbit eyes have unique advantages to serve as this non-rodent, large animal eye model required by the FDA for evaluation of new pharmaceutical therapies. Thus, the rabbit model we developed is particularly important to evaluate new treatments of anti-VEGF resistance in CNV. There are several advantages of having CNV in a large animal eye like a rabbit. Rabbit eyes share many similarities with human eyes including size, vasculature, structure, optical scheme, biochemical and biomechanical makeup. The axial

length of rabbit's eye is 18.1 mm, nearly 80% that of humans (23 mm). Mice eyes have a axial length of 3.2 mm, which is only 14% that of humans (Zhou et al., 2008). Rabbits are larger and have a relatively long lifespan (5–7 years vs. 1.3–3 years in mice), enabling studies of age-related photoreceptor, retinal and RPE degeneration and assessment of long-term therapeutic effects and toxicity (Comfort, 1959). Several physiologic manipulation equipment and therapeutic interventions fabricated for human eyes can be performed in rabbits with slight modification (Fan et al., 2015; Graur et al., 1996; Li et al., 1990; Woodruff-Pak and Trojanowski, 1996; Y Zernii et al., 2016). In previous studies, our group has shown a 100% success rate in creating CNV models using Matrigel/VEGF subretinal injections that stay stable over a month (Li et al., 2019). By using the mouse laser photocoagulation to create CNV, CNV rapidly developed and reached a peak at week 2 with strong fluorescein leakage and then gradual reduction in the following month due to the re-restoration of the blood-retina barrier and the speedy maturation of CNV (Gregor and Ryan, 1982). These impacts make the mouse laser-CNV model more challenging to follow the treatment longitudinally.

Using a multimodal PAM and OCT image acquisition, CNV in both young and old rabbits was detected and visualized with high spatial resolution. This integrated system allows for resolving microvasculature while maintaining light significantly lower than that of the ANSI safety threshold energy level at approximately half the level (~80nJ) (Nguyen et al., 2020; Nguyen et al., 2021b; Tian et al., 2017b; Tian et al., 2018). Compared to frequently used methods of imaging, our system combines two powerful imaging modalities to provide high resolution and clear contrast images of individual blood vessels for improved detection of abnormal and/or diseased capillaries and angiogenesis.

5. Conclusion

In summary, this is the first study conducted to delineate differences in response to bevacizumab between two different age groups of rabbits using a variety of different imaging techniques. The results showed that young rabbits with CNV responded favorably to bevacizumab while older rabbits exhibited minimal response to treatment. This is also the first study to monitor and assess the progression of CNV using integrated PAM and OCT imaging technology in two age groups concurrently. This novel animal model and ophthalmic imaging setup can be a safe and useful tool for visualizing CNV and monitoring the differences in the drug therapy response over time.

Supplementary Material

Refer to Web version on PubMed Central for supplementary material.

Acknowledgments:

This report was sponsored by grants from the National Eye Institute with grant number 1K08EY027458 (YMP), 1R41EY031219 (YMP), 1R01EY033000 (YMP), 1R01EY029489 (YMP and XW), Fight for Sight- International Retinal Research Foundation grant number FFSGIA16002 (YMP), and Alcon Research Institute Young Investigator Grant (YMP). Unrestricted departmental support was also provided by Research to Prevent Blindness and the University of Michigan Department of Ophthalmology and Visual Sciences. This research additionally utilized the Core Center for Vision Research financed by the National Eye Institute grant number P30 EY007003. The

authors thank Dr. Yuqing Chen and the Center for Advanced Models and Translational Sciences and Therapeutics (CAMTraST) at the University of Michigan Medical School for the generous donation of New Zealand rabbits.

References

Abdo M, Haddad S, Emam M, 2017. Development of the New Zealand White Rabbit Eye: I. Pre-and Postnatal Development of Eye Tunics. Anatomia, histologia, embryologia 46, 423–430. [PubMed: 28703411]

Ahn SJ, Hong HK, Na YM, Park SJ, Ahn J, Oh J, Chung JY, Park KH, Woo SJ, 2016. Use of rabbit eyes in pharmacokinetic studies of intraocular drugs. JoVE (Journal of Visualized Experiments), e53878.

Ameri H, Chader GJ, Kim JG, Sadda SR, Rao NA, Humayun MS, 2007. The effects of intravitreous bevacizumab on retinal neovascular membrane and normal capillaries in rabbits. Invest Ophthalmol Vis Sci 48, 5708–5715. [PubMed: 18055823]

Buckle M, Lee A, Mohamed Q, Fletcher E, Sallam A, Healy R, Stratton I, Tufail A, Johnston R, 2015. Prevalence and incidence of blindness and other degrees of sight impairment in patients treated for neovascular age-related macular degeneration in a well-defined region of the United Kingdom. Eye 29, 403–408. [PubMed: 25592123]

Cao J, Zhao L, Li Y, Liu Y, Xiao W, Song Y, Luo L, Huang D, Yancopoulos GD, Wiegand SJ, 2010. A subretinal matrigel rat choroidal neovascularization (CNV) model and inhibition of CNV and associated inflammation and fibrosis by VEGF trap. Investigative ophthalmology & visual science 51, 6009–6017. [PubMed: 20538989]

Cheung CMG, Arnold JJ, Holz FG, Park KH, Lai TY, Larsen M, Mitchell P, Ohno-Matsui K, Chen S-J, Wolf S, 2017. Myopic choroidal neovascularization: review, guidance, and consensus statement on management. Ophthalmology 124, 1690–1711. [PubMed: 28655539]

Cohen SY, Laroche A, Leguen Y, Soubrane G, Coscas GJ, 1996. Etiology of choroidal neovascularization in young patients. Ophthalmology 103, 1241–1244. [PubMed: 8764794]

Comfort A, 1959. Natural aging and the effects of radiation. Radiation Research Supplement 1, 216–234.

Del Amo EM, Urtti A, 2015. Rabbit as an animal model for intravitreal pharmacokinetics: Clinical predictability and quality of the published data. Experimental eye research 137, 111–124. [PubMed: 25975234]

Fan J, Kitajima S, Watanabe T, Xu J, Zhang J, Liu E, Chen YE, 2015. Rabbit models for the study of human atherosclerosis: from pathophysiological mechanisms to translational medicine. Pharmacology & therapeutics 146, 104–119. [PubMed: 25277507]

Ferris FL, Fine SL, Hyman L, 1984. Age-related macular degeneration and blindness due to neovascular maculopathy. Archives of ophthalmology 102, 1640–1642. [PubMed: 6208888]

Graur D, Duret L, Gouy M, 1996. Phylogenetic position of the order Lagomorpha (rabbits, hares and allies). Nature 379, 333–335. [PubMed: 8552186]

Gregor Z, Ryan SJ, 1982. Blood-retinal barrier after blunt trauma to the eye. Graefe's Archive for Clinical and Experimental Ophthalmology 219, 205–208.

Hasumura T, Yonemura N, Hirata A, Murata Y, Negi A, 2000. Retinal damage by air infusion during vitrectomy in rabbit eyes. Investigative ophthalmology & visual science 41, 4300–4304. [PubMed: 11095630]

Johnson CJ, Berglin L, Chrenek MA, Redmond T, Boatright JH, Nickerson JM, 2008. Technical brief: subretinal injection and electroporation into adult mouse eyes. Molecular vision 14, 2211. [PubMed: 19057658]

Kiilgaard JF, Andersen MVN, Wiencke AK, Scherfig E, La Cour M, Tezel TH, Prause JU, 2005. A new animal model of choroidal neovascularization. Acta Ophthalmologica Scandinavica 83, 697–704. [PubMed: 16396647]

Li W-H, Gouy M, Sharp PM, O'hUigin C, Yang Y-W, 1990. Molecular phylogeny of Rodentia, Lagomorpha, Primates, Artiodactyla, and Carnivora and molecular clocks. Proceedings of the National Academy of Sciences 87, 6703–6707.

Li Y, Zhang W, Nguyen VP, Rosen R, Wang X, Xia X, Paulus YM, 2019. Real-time OCT guidance and multimodal imaging monitoring of subretinal injection induced choroidal neovascularization in rabbit eyes. Experimental eye research 186, 107714. [PubMed: 31288022]

Lima LH, Farah ME, Gum G, Ko P, de Carvalho RA, 2018. Sustained and targeted episcleral delivery of celecoxib in a rabbit model of retinal and choroidal neovascularization. International Journal of Retina and Vitreous 4, 31. [PubMed: 30116590]

Maguire M, Martin D, Ying G, Jaffe G, Daniel E, Grunwald J, Toth C, Ferris F 3rd, Fine S, 2016. Comparison of Age-related Macular Degeneration Treatments Trials (CATT) Research Group Five-year outcomes with anti-vascular endothelial growth factor treatment of neovascular age-related macular degeneration: the comparison of age-related macular degeneration treatments trials. Ophthalmology 123, 1751–1761. [PubMed: 27156698]

Martin DF, Maguire MG, Ying G, Grunwald JE, Fine SL, Jaffe GJ, 2011. Ranibizumab and bevacizumab for neovascular age-related macular degeneration. The New England journal of medicine 364, 1897–1908. [PubMed: 21526923]

Mettu PS, Allingham MJ, Cousins SW, 2021. Incomplete response to Anti-VEGF therapy in neovascular AMD: Exploring disease mechanisms and therapeutic opportunities. Progress in Retinal and Eye Research 82, 100906. [PubMed: 33022379]

Miller H, Miller B, Ishibashi T, Ryan SJ, 1990. Pathogenesis of laser-induced choroidal subretinal neovascularization. Investigative ophthalmology & visual science 31, 899–908. [PubMed: 1692312]

Mukesh BN, Dimitrov PN, Leikin S, Wang JJ, Mitchell P, McCarty CA, Taylor HR, 2004. Five-year incidence of age-related maculopathy: the Visual Impairment Project. Ophthalmology 111, 1176–1182. [PubMed: 15177968]

Nguyen CL, Oh LJ, Wong E, Wei J, Chilov M, 2018. Anti-vascular endothelial growth factor for neovascular age-related macular degeneration: a meta-analysis of randomized controlled trials. BMC ophthalmology 18, 1–15. [PubMed: 29301512]

Nguyen V-P, Li Y, Henry J, Zhang W, Aaberg M, Jones S, Qian T, Wang X, Paulus YM, 2020. Plasmonic gold nanostar-enhanced multimodal photoacoustic microscopy and optical coherence tomography molecular imaging to evaluate choroidal neovascularization. ACS sensors 5, 3070–3081. [PubMed: 32921042]

Nguyen V-P, Li Y, Henry J, Zhang W, Wang X, Paulus YM, 2021a. Gold Nanorod Enhanced Photoacoustic Microscopy and Optical Coherence Tomography of Choroidal Neovascularization. ACS Applied Materials & Interfaces 13, 40214–40228. [PubMed: 34403578]

Nguyen VP, Fan W, Zhu T, Qian W, Li Y, Liu B, Zhang W, Henry J, Yuan S, Wang X, 2021b. Long-Term, Noninvasive In Vivo Tracking of Progenitor Cells Using Multimodality Photoacoustic, Optical Coherence Tomography, and Fluorescence Imaging. ACS nano 15, 13289–13306. [PubMed: 34378374]

Nguyen VP, Qian W, Li Y, Liu B, Aaberg M, Henry J, Zhang W, Wang X, Paulus YM, 2021c. Chain-like gold nanoparticle clusters for multimodal photoacoustic microscopy and optical coherence tomography enhanced molecular imaging. Nature Communications 12, 1–14.

Qiu G, Stewart JM, Sadda S, Freda R, Lee S, Guven D, de Juan E Jr, Varner SE, 2006. A new model of experimental subretinal neovascularization in the rabbit. Experimental eye research 83, 141–152. [PubMed: 16579984]

Reichenbach A, Schnitzer J, Friedrich A, Knothe AK, Henke A, 1991a. Development of the rabbit retina: II. Müller cells. Journal of Comparative Neurology 311, 33–44. [PubMed: 1939735]

Reichenbach A, Schnitzer J, Friedrich A, Ziegert W, Brückner G, Schober W, 1991b. Development of the rabbit retina. Anatomy and embryology 183, 287–297. [PubMed: 2042753]

Rein DB, Wittenborn JS, Zhang X, Honeycutt AA, Lesesne SB, Saaddine J, Group VHC-ES, 2009. Forecasting age-related macular degeneration through the year 2050: the potential impact of new treatments. Archives of ophthalmology 127, 533–540. [PubMed: 19365036]

Semkova I, Peters S, Welsandt G, Janicki H, Jordan J, Schraermeyer U, 2003. Investigation of laser-induced choroidal neovascularization in the rat. Investigative ophthalmology & visual science 44, 5349–5354. [PubMed: 14638737]

Shah RS, Soetikno BT, Lajko M, Fawzi AA, 2015. A mouse model for laser-induced choroidal neovascularization. JoVE (Journal of Visualized Experiments), e53502. [PubMed: 26779879]

Solomon SD, Lindsley K, Vedula SS, Krzystolik MG, Hawkins BS, 2014. Anti-vascular endothelial growth factor for neovascular age-related macular degeneration. Cochrane Database of Systematic Reviews.

Stem MS, Moinuddin O, Kline N, Thanos A, Rao P, Williams GA, Hassan TS, 2018. Outcomes of anti–vascular endothelial growth factor treatment for choroidal neovascularization in fellow eyes of previously treated patients with neovascular age-related macular degeneration. JAMA ophthalmology 136, 820–823. [PubMed: 29800991]

Tian C, Zhang W, Mordovanakis A, Wang X, Paulus YM, 2017a. Noninvasive chorioretinal imaging in living rabbits using integrated photoacoustic microscopy and optical coherence tomography. Opt Express 25, 15947–15955. [PubMed: 28789105]

Tian C, Zhang W, Mordovanakis A, Wang X, Paulus YM, 2017b. Noninvasive chorioretinal imaging in living rabbits using integrated photoacoustic microscopy and optical coherence tomography. Optics express 25, 15947–15955. [PubMed: 28789105]

Tian C, Zhang W, Nguyen VP, Wang X, Paulus YM, 2018. Novel photoacoustic microscopy and optical coherence tomography dual-modality chorioretinal imaging in living rabbit eyes. JoVE (Journal of Visualized Experiments), e57135.

Wong WL, Su X, Li X, Cheung CMG, Klein R, Cheng C-Y, Wong TY, 2014. Global prevalence of age-related macular degeneration and disease burden projection for 2020 and 2040: a systematic review and meta-analysis. The Lancet Global Health 2, e106–e116. [PubMed: 25104651]

Woodruff-Pak DS, Trojanowski JQ, 1996. The older rabbit as an animal model: implications for Alzheimer's disease. Neurobiology of aging 17, 283–290. [PubMed: 8744410]

Y Zernii E, E Baksheeva V, N Iomdina E, A Averina O, E Permyakov S, P Philippov P, A Zamyatnin A, I Senin I, 2016. Rabbit models of ocular diseases: new relevance for classical approaches. CNS & Neurological Disorders-Drug Targets (Formerly Current Drug Targets-CNS & Neurological Disorders) 15, 267–291.

Zhang W, Li Y, Nguyen VP, Derouin K, Xia X, Paulus YM, Wang X, 2020a. Ultralow energy photoacoustic microscopy for ocular imaging in vivo. Journal of Biomedical Optics 25, 066003. [PubMed: 32519521]

Zhang W, Li Y, Nguyen VP, Huang Z, Liu Z, Wang X, Paulus YM, 2018. High-resolution, in vivo multimodal photoacoustic microscopy, optical coherence tomography, and fluorescence microscopy imaging of rabbit retinal neovascularization. Light: Science & Applications 7, 1–12.

Zhang W, Li Y, Yu Y, Derouin K, Qin Y, Nguyen VP, Xia X, Wang X, Paulus YM, 2020b. Simultaneous photoacoustic microscopy, spectral-domain optical coherence tomography, and fluorescein microscopy multi-modality retinal imaging. Photoacoustics 20, 100194. [PubMed: 32566480]

Zhou X, Xie J, Shen M, Wang J, Jiang L, Qu J, Lu F, 2008. Biometric measurement of the mouse eye using optical coherence tomography with focal plane advancement. Vision research 48, 1137–1143. [PubMed: 18346775]

Zhu L, Parker M, Enemchukwu N, Shen M, Zhang G, Yan Q, Handa JT, Fang L, Fu Y, 2020. Combination of apolipoprotein-AI/apolipoprotein-AI binding protein and anti-VEGF treatment overcomes anti-VEGF resistance in choroidal neovascularization in mice. Communications biology 3, 1–11. [PubMed: 31925316]

Highlights:

1. Comparison of choroidal neovascularization (CNV) in young and aged large animal models using bevacizumab (Bev), an anti-vascular endothelial growth factor (VEGF) medication, treatment is described as a novel method to demonstrate persistent disease activity and evaluate the efficiency of Bev in different ages of animals.
2. There is a significant difference in response to intravitreal bevacizumab treatment between young and old rabbits with CNV which can be monitored with multimodal molecular imaging.
3. Robust CNV developed in both young and old rabbits by subretinal injection of VEGF and Matrigel with a 100% success rate.
4. CNV was reduced by more than 90% after intravitreal bevacizumab injection in young rabbits (4 months old) while life-span rabbits (14 months old) demonstrate significant persistent disease activity with only 10.6% reduction in CNV post-bevacizumab treatment.
5. CNV treatment can be monitored by a multimodal, non-invasive, high resolution photoacoustic microscopy (PAM), optical coherence tomography (OCT), and fluorescence imaging.
6. OCT images confirmed a rapid decrease of CNV in the young group.
7. Contrast agents (ultrapure chain-like gold nanoparticle clusters) demonstrated high PAM signal in old rabbits and minimal PAM signal in young rabbits after bevacizumab, indicating CNV regression.

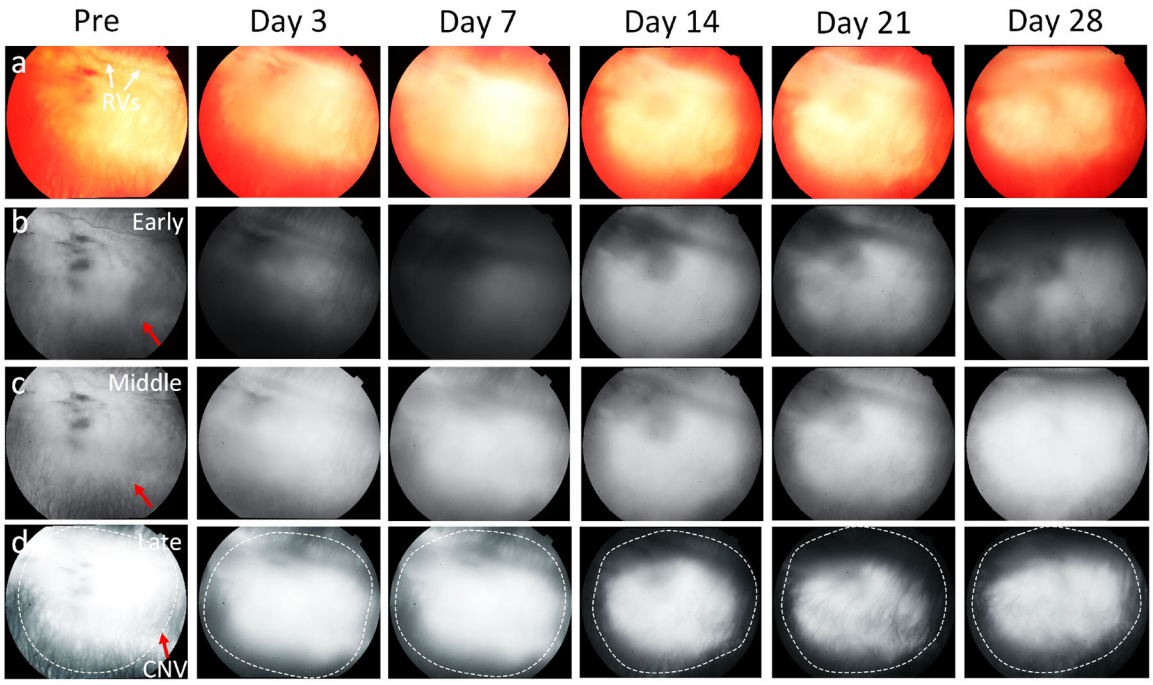

Figure 1. ***In vivo*** **monitoring of CNV in rabbit model without treatment with Avastin:**
(a) Color fundus photography obtained at 3, 7, 14, 21, and 28 days post subretinal injection of VEGF. (b-d) Early, middle, and late phase FA images. CNV density were not significantly changed over time.

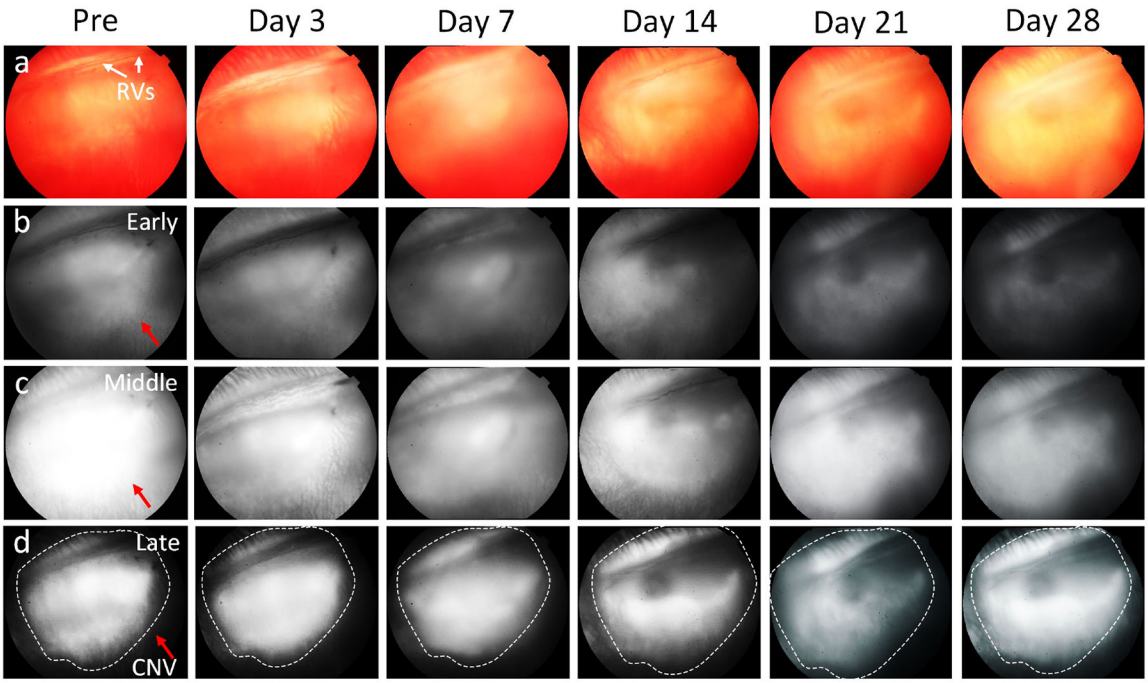

Figure 2. Intravitreal injection of BEV old rabbit models (14 months old):
(a) Color images. (b-d) FA images of the rabbit captured at early phase (b), middle phase (c) and late phase (d) pre and post treatment. The late phase FA images shows leakage consistent with CNV membrane. The rabbit with CNV models received intravitreal BEV 1.25 mg in the left eye. At day 28 post treatment, no significant therapeutic effect was observed with continued significant late leakage on FA.

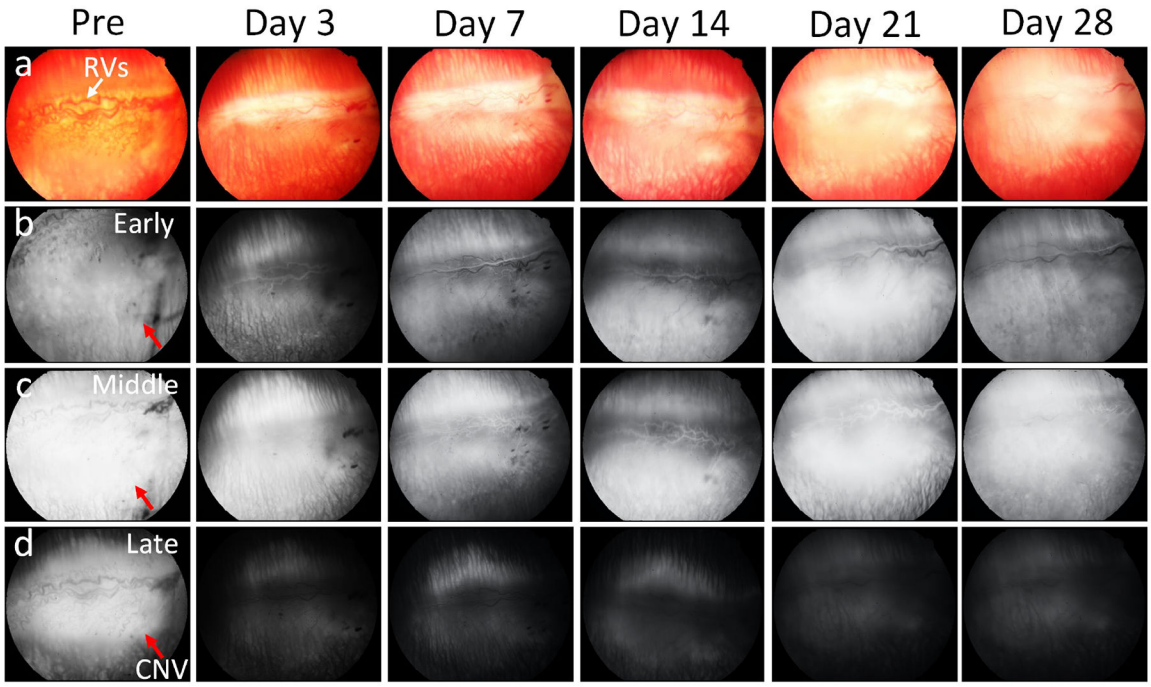

Figure 3. Visualization of choroidal neovascularization (CNV) progression followed bevacizumab (BEV) treatment on young rabbit model (4 months old):

(a) Color fundus photography. (b-d) Fluorescein angiography images achieved at early phase (b), middle phase (c) and late phase (d) pre and post BEV administration at days 3, 7, 14, 21 and 28, respectively. The rabbit with CNV models received intravitreal BEV 1.25 mg in the left eye. The retinal morphology was become normal at day 28 post therapy. Noted that CNV activity had significantly reduced.

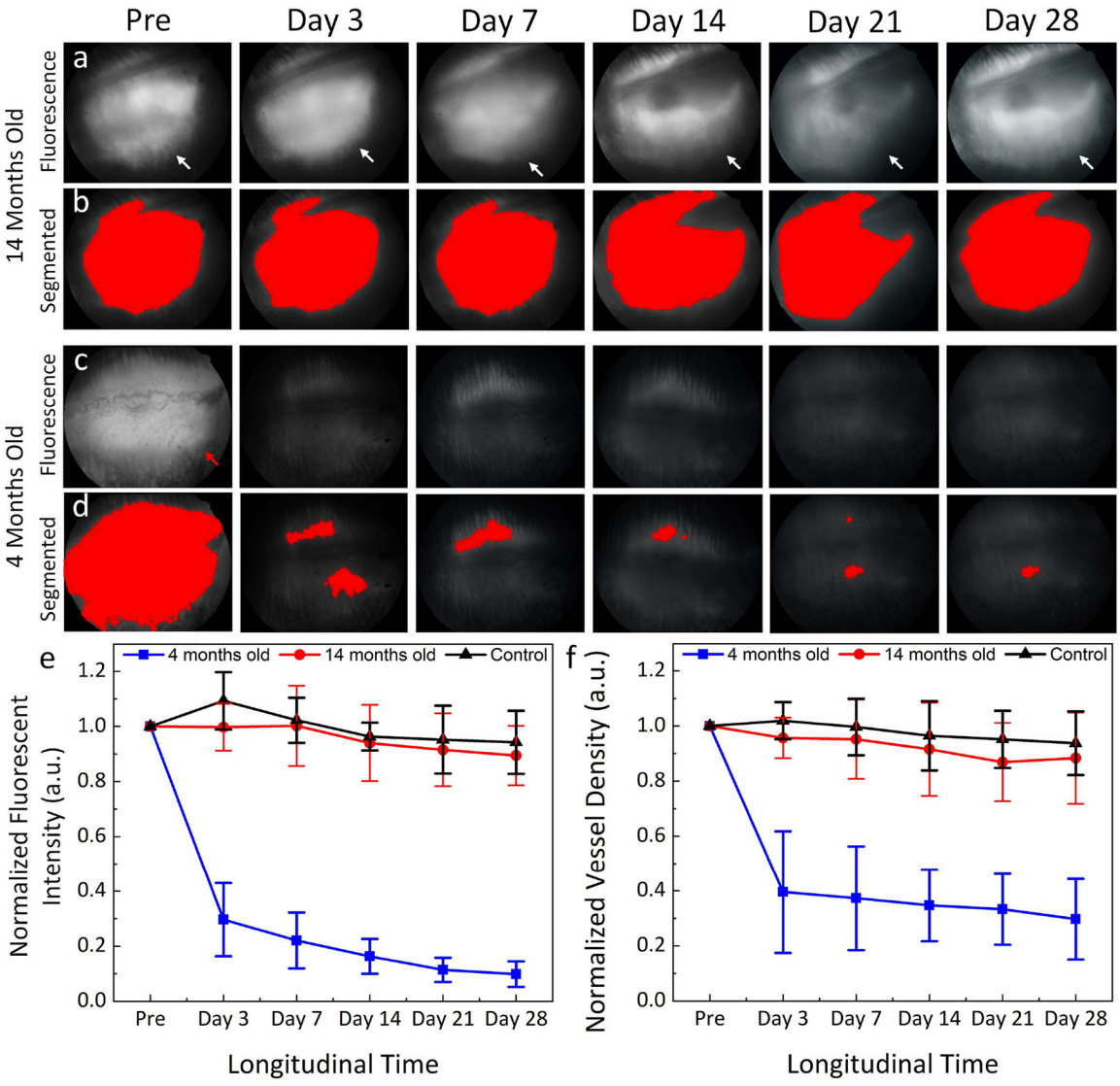

Figure 4. Image segmentation and statistical analysis of the CNV density after treatment:
(a-b) FA images and the segmented CNV area of the 14 months old group (n = 3). (c-d) FA images and the segmented CNV area of the 4 months old group (n = 3). (e) Graph of the normalized fluorescent intensity measured from three different BEV treatment groups: 4 months, 14 months, and control groups (no BEV treatment). (f) Quantitative normalized vessel density (n=3), *p< 0.005 compared to the untreated group using ANOVA.

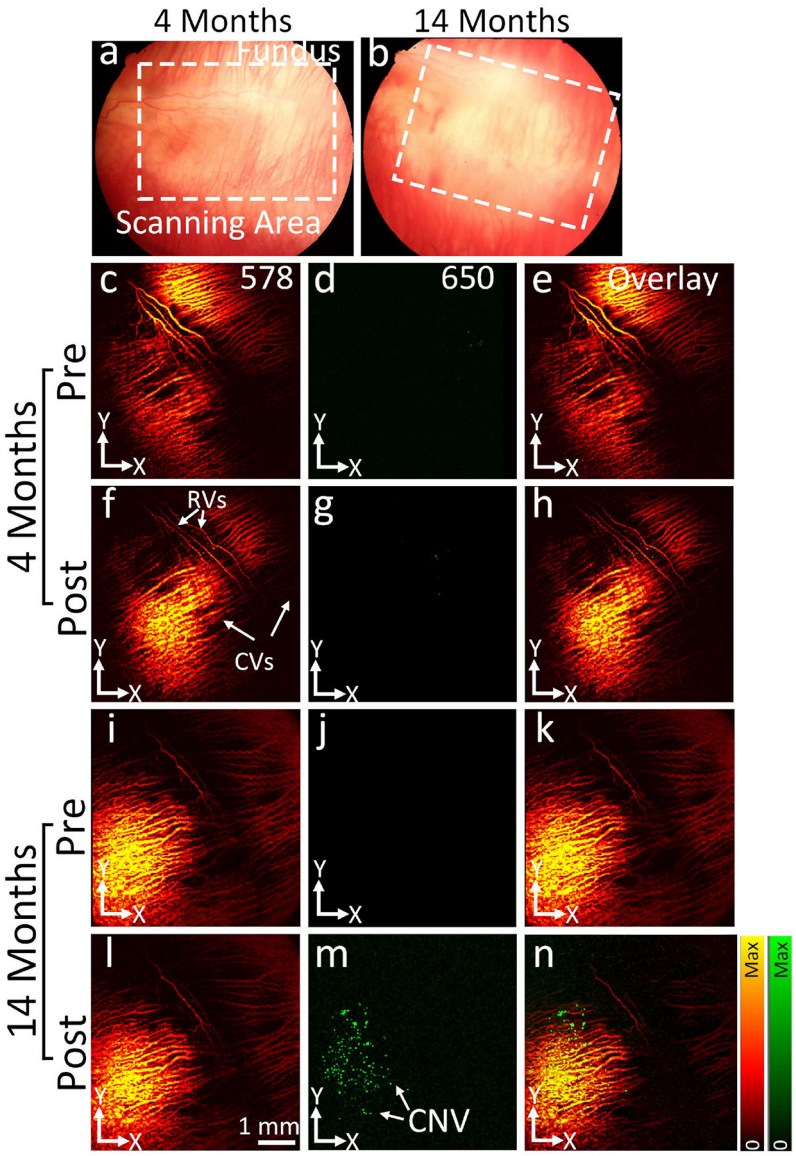

Figure 5. ***In vivo*** **PAM images of CNV post treatment:**

(a-b) Color fundus photographs of 4- and 14-months rabbits post treatment at day 28. (c-h) and (i-n) PAM images achieved at 578 and 650 nm pre and post administration of CGNPs (400 μg/mL, 5 mg/mL). The location of CGNP binding at CNV was pointed out by green color. (d-h) Overlay PAM images.

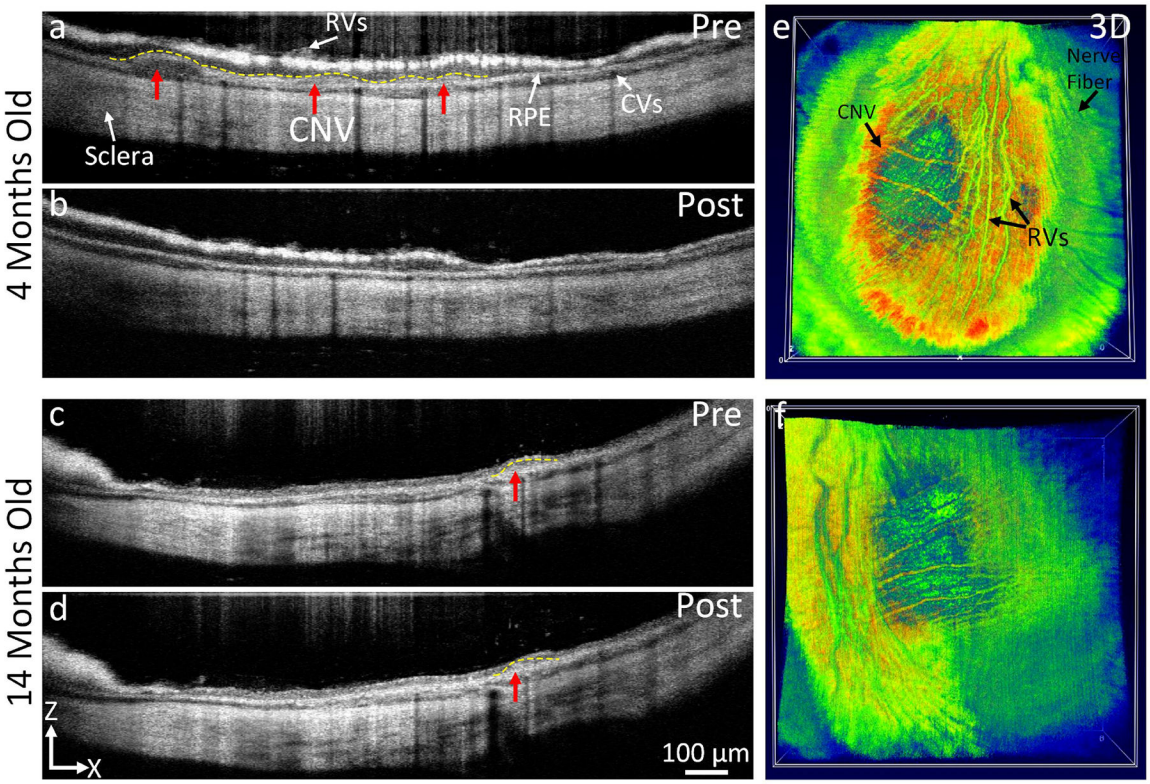

Figure 6. ***In vivo*** **OCT visualization of CNV in rabbit models:**

(a-c) OCT image before treatment in 4 months and 14 moths rabbit models shows an indistinct area of CNV (red arrow and dotted yellow line) under subretinal space. No CNV was observed on the OCT post treatment at day 28 (b). In contrast, CNV was clearly observed on the OCT image acquired from 14 months rabbits (d). (e-f) 3D OCT images.

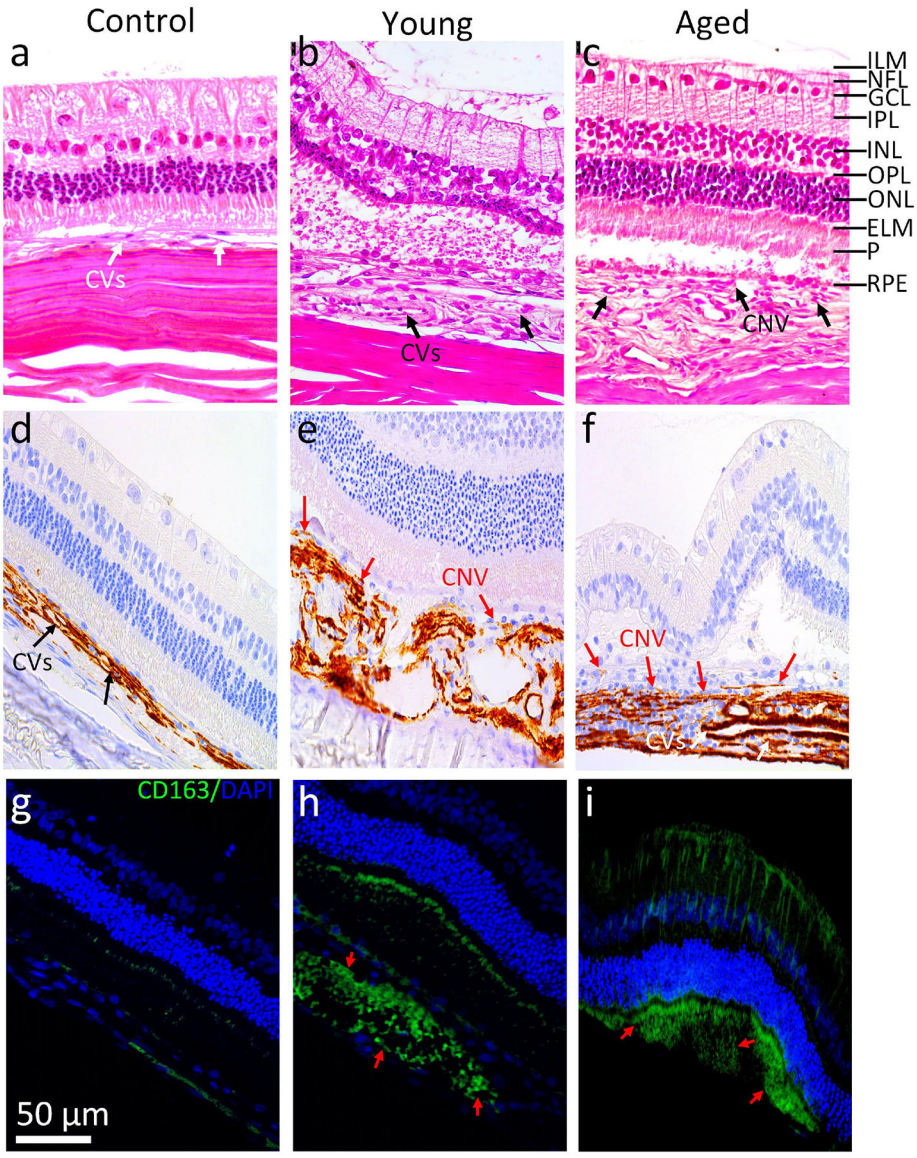

Figure 7. Histological Evaluation of CNV on day 28:

(a) Control eye, (b) BEV treatment on 4 months rabbits, and BEV treatment on 14 months rabbits (c). Pathologic choroidal vessels are display in the control eye (white arrow) as shown in a. Both blood vessels and neovascularization are visible (black arrows) in the region of newly developed CNV 28 days post treatment of BEV as shown in b and c. (d-f) IHC images of control, 4 months, and 14 months groups with a-SMA labeling. (g-i) Immunofluorescence images of cross sections obtained from control, young and aged rabbits. Blue fluorescence indicates nuclei stained with DAPI. Green emission fluorescence signal represents CD163-activated macrophages (red arrows) that are not present in control but are present in both 4 months and 14 months groups. Scale bar is 50 µm.